P9.2 Radar Image Segmentation Using Active Contour Method

Pengfei Zhang[*1], and Meijun Zhu[2]
[1]CIMMS, University of Oklahoma, Norman, Oklahoma
[2]Departmenyt of Mathematics, University of Oklahoma, Norman, Oklahoma

1. Introduction

Weather radar data quality control is extremely important for meteorological and hydrological applications. For weather radars, scatterers in the atmosphere are not only meteorological particles like cloud, rain drops, snowflakes, and hails, but also non-meteorological particles such as chaff, insects, and birds. For radar meteorologists it is a major issue and challenge to design numerical scheme which can automatically and subjectively distinguish meteorological echoes from non-meteorological echoes. Non-meteorological echoes can contaminate radar reflectivity and Doppler velocity measurements, and subsequently cause errors and uncertainty on radar data applications in quantitative precipitation estimation, as well as in assimilation in numerical model for weather prediction. Automatic detection of tornado or mesocyclone vortex among meteorological echoes is certainly another big challenge and has great potential in improving severe weather forecast and saving human life.

Many algorithms such as fuzzy logic, and neural network, have been developed to distinguish different echoes observed by the weather radars in order to control the data quality for diverse applications (Kessinger et al., 2003, Lakshmanan et al., 2007, Zhang et al., 2005).

The graphic properties such as pattern, intensity and texture of echoes are commonly used in those algorithms. Active contour is another pattern recognition method that seeks the boundary of desired feature. This method has been widely used on image processing in many fields, but not in radar image processing yet. We have modified Chan-Vese method and tested it on several radar images containing typical weather patterns like tornadic supercell, snow, squall line, and etc.

2. Methodology

Active contour is the procedure that we deform a given curve so that a given functional of the curve will achieve its local minimal value. Recently, this method is wildly used in seeking the edges or contours of given images (Mumford and Shah, 1989; Kass, et al., 1987; Caselles, et al., 1997; Chan and Vese, 2001). Let $u_0(x, y)$ be the gray level function of a given image. Assume that the image u_0 is formed by two regions with different intensities and textures. Also assume these two regions can be distinguished by a closed curve C. If u_0 is smooth, then $|\nabla u_0|$ should be relatively large along the boundary between these regions. So we introduce the following modified Chan-Vese energy based-segmentation functional:

$$I(C,c) = \int |u_0 - \alpha \cdot M|^2 \, dxdy + \int |u_0 - c|^2 \, dxdy + \mu(length(C) + \nu(area(inside(C))), \quad (1)$$

*Corresponding author address: Pengfei Zhang, CIMMS, University of Oklahoma, Norman, OK 73072; e-mail: pengfei.zhang@noaa.gov

where M=max(u_o) , c is the averages of u_o outside C, α, μ, and ν are fixed parameters. Embedding C as a nodal line of a smooth function $\Phi(x,y,t)$: $C=\{(x,y,t):\Phi(x,y,t)=0\}$, we can rewrite the Eq.(1) as

$$J(\Phi,c)=\int_{\Omega}|u_0-\alpha\cdot M|^2\,H(\Phi(x,y))dxdy+\int_{\Omega}|u_0-c|^2\,(1-H(\Phi(x,y)))dxdy$$
$$+\mu\int_{\Omega}\delta(\Phi(x,y))|\nabla\Phi(x,y)|\,dxdy+\nu\int_{\Omega}H(\Phi(x,y))dxdy \quad , \qquad (2)$$

where H and δ are step function and delta function respectively, t is artificial time and always larger than zero for parameterizing the decent direction. Here slightly regularized version of functions H_ε and $H_\varepsilon^{'}=\delta_\varepsilon$ such that $H_\varepsilon = H$ and $\delta_\varepsilon=\delta$ as ε approaching to 0. Then the Eq.(2) becomes

$$J(\Phi,c)=\int_{\Omega}|u_0-\alpha\cdot M|^2\,H_\varepsilon(\Phi(x,y))dxdy+\int_{\Omega}|u_0-c|^2\,(1-H_\varepsilon(\Phi(x,y)))dxdy$$
$$+\mu\int_{\Omega}\delta_\varepsilon(\Phi(x,y))|\nabla\Phi(x,y)|\,dxdy+\nu\int_{\Omega}H_\varepsilon(\Phi(x,y))dxdy \quad . \qquad (3)$$

Minimizing J via deforming Φ along its gradient direction with fixed α and c:

$$\frac{\partial\Phi}{\partial t}=\delta_\varepsilon(\Phi)[\mu\cdot div(\frac{\nabla\Phi}{|\nabla\Phi|})-\nu-(u_0-\alpha\cdot M)^2+(u_0-c)^2] \quad , \qquad (4)$$

$$\Phi(x,y,0)=\Phi_0(x,y) \quad , \qquad (5)$$

$$\frac{\delta_\varepsilon(\Phi)}{|\nabla\Phi|}\frac{\partial\Phi}{\partial n}=0 \quad , \qquad (6)$$

where $\vec{n}$ denotes exterior normal to the curve C. Eq.(5) and Eq.(6) are initial and boundary conditions respectively. By integrating Eq.(4) for a certain time, function Φ will reach to a stable stage. At this time, the region inside contour Φ(x,y)=0 is the desired region. More detailed derivations can be found in Chan and Vese (2001) paper.

Note that μ in the Eq.(4) controls the contraction/expansion speed and the roundness of the curve C. If we want to detect small scale features, then μ should be relatively small. On the other hand, if we only focus on large scale features, then μ should be relatively large. α controls the closeness to the maximum intensity of the desired feature.

3. Experimental results

In our experiments, active contour method is applied to different radar reflectivity images observed by operational WSR-88D radar to segment weather echoes from clear air echoes and ground clutters. Three different weather phenomena such as squall line, tornadic super cell, and stratiform rain are selected to examine the performance of the method. For all the following experiments presented in this paper, parameter ν in the Eq.(4) was set to zero. But μ and α vary in the different experiments.

A squall line was observed by KTLX radar at 00:20 UTC on 31 March 2009. A disk like clear air echo was contiguous to the squall line around the radar. Fig.1 shows the reflectivity factor field at the elevation angle of 0.5^o in gray level at that time. The evolution of the active contour Φ (solid blue curve) is also presented in Fig.1. The initial condition of the contour is a square showed in Fig.1a. It can be seen that the contour Φ gradually converge to the feature (i.e. squall line) with high gray level and blur boundary. Comparing Fig.1e and f, we found that there is no obvious difference between them. It implies that the contour reaches its stable stage at integration step of 2100. Around this time, the right hand side of Eq.(4) approaches to zero, and energy function J reach to its minimum. Technically, integration of Eq.(4) in the numerical model stopped at step of 2500. Note that the active contour can not only contract to the desired feature as seen in its evolution but also expand itself. The contour near the top of the squall line actually expanded to the edge of the image at the step of 500 (Fig.1a and 1b) and stayed there until the end of integration.

Fig.2 shows the reflectivity field of a tornadic super cell and thunderstorms observed by KTLX at elevation angle of 0.5^o at 00:27 UTC on 4 May 1999. Clearly, the super cell and thunderstorm echoes are embedded in ground clutter around the radar (black dot right below the super cell) and a disc-like clear echo with relatively weak intensity. The inputs of the numerical model in the following experiments are the images in gray level (not shown) like Fig.1. The color images showed in Fig.2 and 3 are only for better visual illustration.

The initial condition is the same as in the first experiment. In order to separate strong large scale super cell and thunderstorm echoes from the small scale ground clutter with strong intensity (>20 dBZ) and large scale clear air echo with weak intensity (~ 13 dBZ), the parameters α and μ are changed to 0.75 and 1.2 respectively. As we mentioned in the previous section, the active contour becomes smoother when it converge to large scale features (Fig.2b). It can be seen that the contour splits into two closed curves (Fig.2c) and then into 3 curves (Fig.2d). This demonstrates the advantages of active contour method that allows automatically change of topology. At the step of 1000 (Fig.2c), the ground clutter is still inside the blue curve, and then becomes outside as the contour continuously converge to the super cell and thunderstorms.

Fig.3 shows a cluster of storm echoes on the right side of the image and half disc of clear air echo near the center of the image. It was observed by KTLX radar at the elevation angle of 0.5^o at 23:04 UTC ON 16 September 2009. This experiment is more challenger than previous two, because the intensity of the clear air echo is just slightly weaker than the one of storm echoes. Furthermore, the clear air echo and storm echoes are merged together. Thus, α is set to 1.0 to let the contour converge to its inside maximum as close as possible. Meanwhile, μ is set to 0.2 in order to detect small scale features of storm echoes. The result exhibits that the most of cluster of storm echoes are successfully distinguished from the clear air echo, although some of small storms near the left and right edges of the image and some echoes at the edge of the storms are excluded by the contour. Comparing with Fig.2d, small wiggles along the contour in Fig.3d shows the effects of small value of μ.

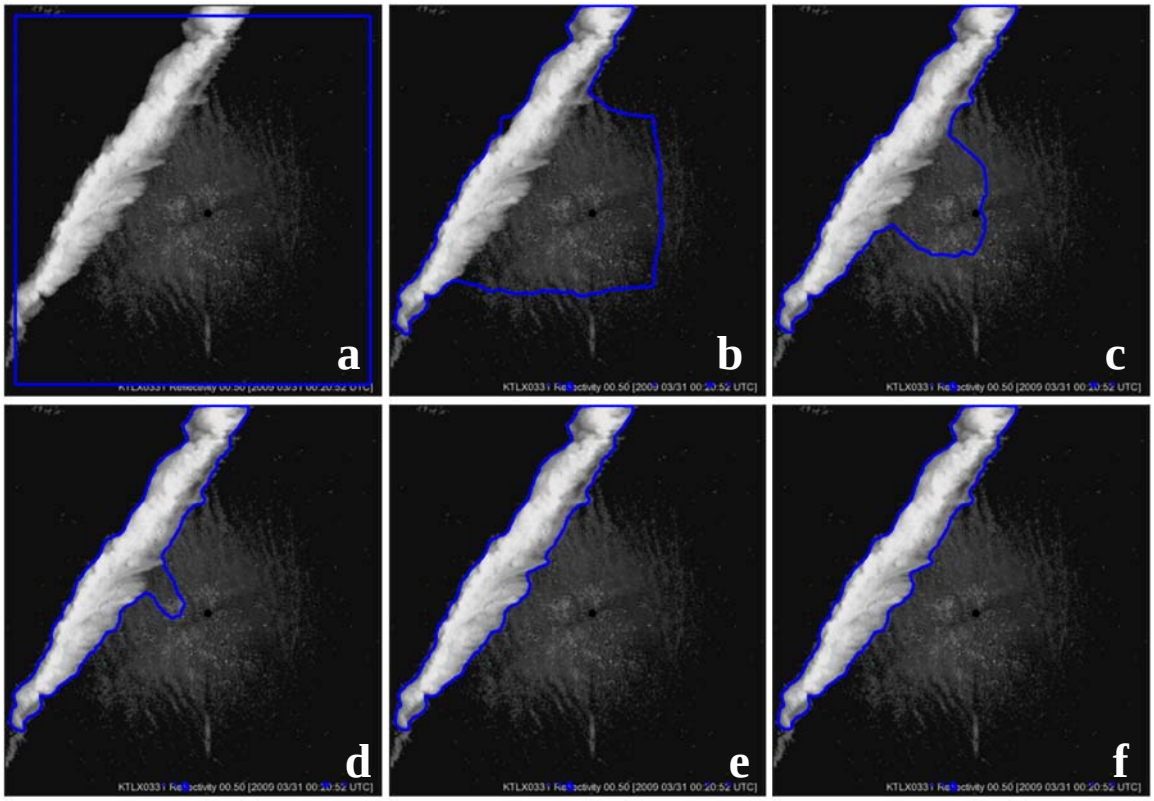

Fig.1 Segmentation of a squall line from clear air echoes. The blue solid curve represents the status of the active contour at integration step of a) 0, b) 500, c) 1000, d) 1500, e) 2100, and f) 2500. Parameters α=0.6, and μ=0.4 for this experiment.

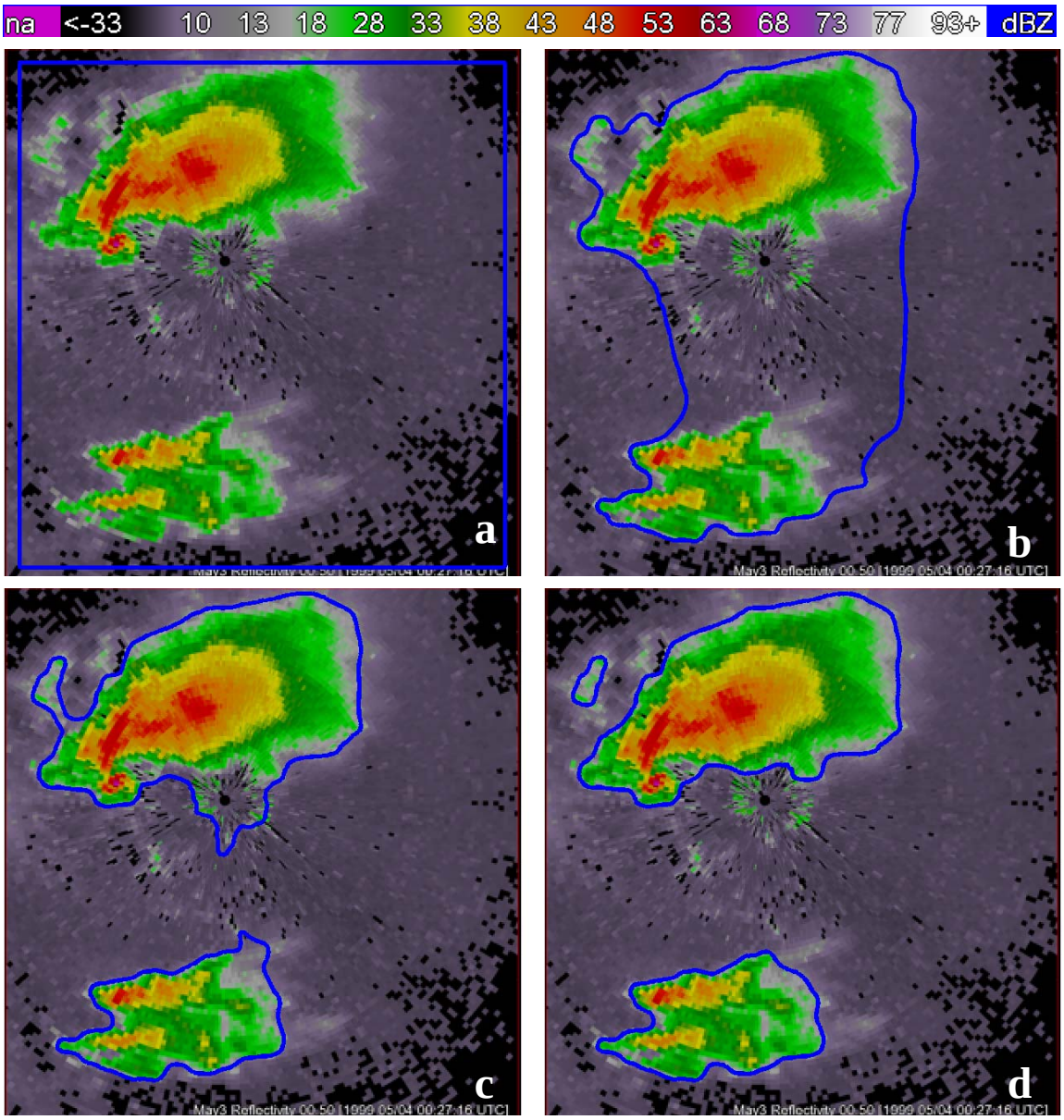

Fig.2 Segmentation of a super cell and thunderstorm from clear air echoes and ground clutter. The blue solid curve represents the status of the active contour at integration step of a) 0, b) 500, c) 1000, and d) 2000. Parameters α=0.75, and μ=1.2 for this experiment.

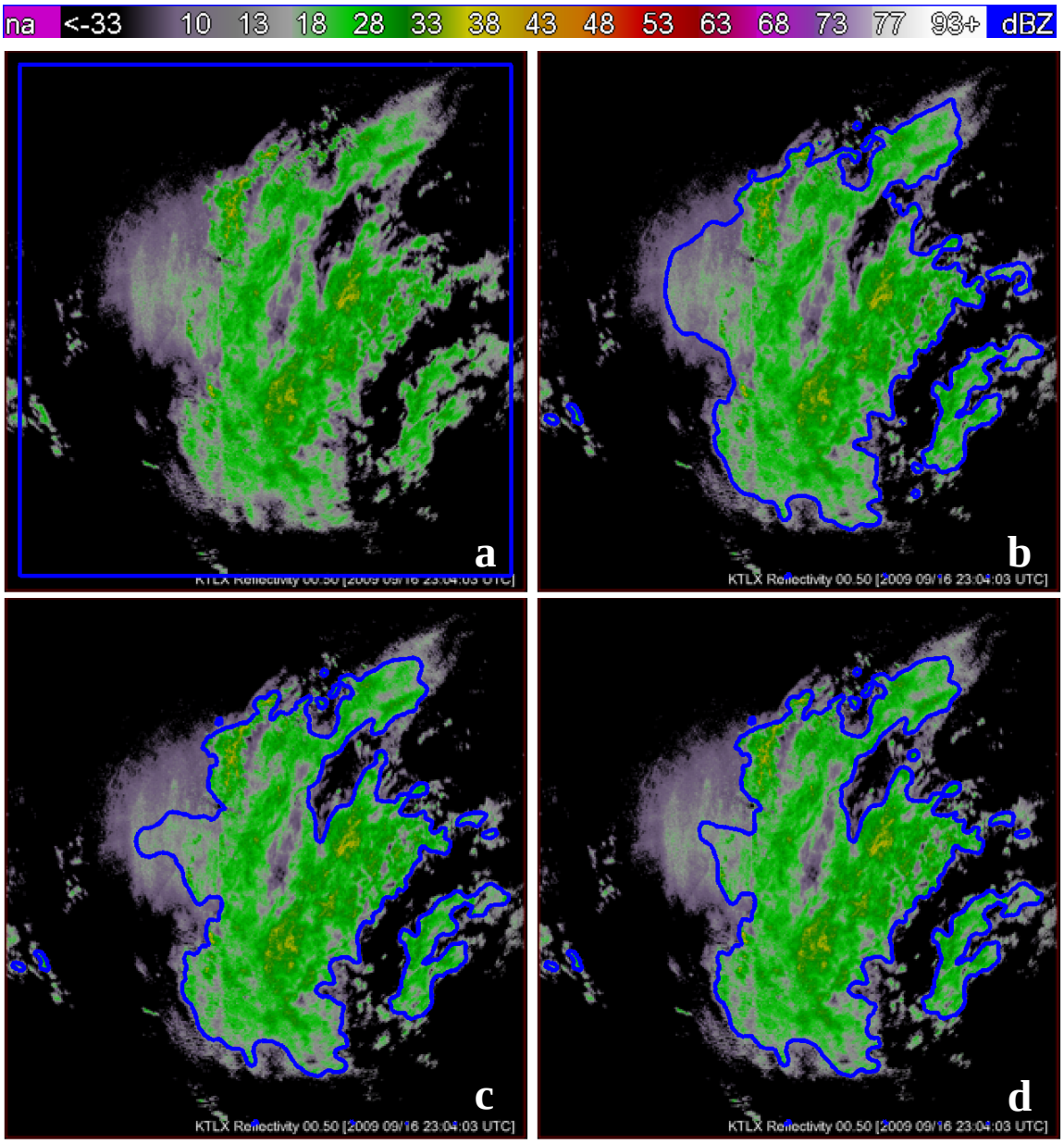

Fig.3 Segmentation of stratiform rain from clear air echoes. The blue solid curve represents the status of the active contour at integration step of a) 0, b) 500, c) 1000, and d) 2500. Parameters α=1.0, and μ=0.2 for this experiment.

It is worth mentioning that active contour is different from conventional contour because the entire properties (i.e. energy defined in Eq.(1)) inside and outside of the active contour are considered. Fig.1f, Fig.2d, and Fig.3d clearly indicate the area wrapped by the active contour is not the area with its intensity larger than certain value at the end of integrations. Actually, the contour groups the areas with common property together.

4. Conclusions and discussions

Active contour method have been modified and applied to the weather radar images for the first time. The results presented in this paper demonstrate that the modified active contour method can be used to distinguish weather echoes from the non-meteorological echoes such as ground clutter and clear air echoes. Certainly, more experiments are needed to examine the robustness of the method. The results have also exhibited the potential of using this method on radar data quality control for operational purpose, in the case automatically finding the appropriate values of parameters α and μ in the numerical model for the images (i.e. data) with different features is still a big challenge.

Reference

Caselles, V., R. Kimmel, and G. Sapiro, 1997: Geodesic active contours, *Int. Journal of Computer Vision*, **22**, no. 1, 61-79.

Chan T., and L. Vese, 2001: Active contours without edges, *IEEE Transactions on Image Processing*, **vol. 10**, no. 2, 266-277.

Kass, M., A. Witkin, and D. Terzopoulos, 1987: Snakes: active contour models, *Int. Journal of Computer Vision*, **1**, 321-331.

Kessinger C., S. Ellis, and J. Van Andel, 2003: The radar echo classifier: A fuzzy logic algorithm for the WSR-88D. Preprints, *Third Conf. on Artificial Applications to the Environmental Sciences*, Long Beach, CA, Amer. Meteor. Soc., CD-ROM, P1.6.

Lakshmanan, V., A. Fritz, T. Smith, K. Hondl, and G. J. Stumpf, 2007: An automated technique to quality control radar reflectivity data. *J. Applied Meteorology*, **46**, 288-305.

Mumford, D., and J. Shah, 1989: Optimal approximations by piecewise smooth functions and associated variational problems. *Comm. Pure Appl. Math.,* **42**, no. 5, 577-685.

Osher, S., and J. Sethian, 1988: Fronts propagating with curvature-dependent speed: algorithms based on Hamilton-Jacobi formulations. *J. Comput. Phys,.* **79**, no. 1, 12-49.

Zhang, P., S. Liu, Q. Xu, 2005: Quality control of Doppler velocities contaminated by migrating birds. Part I: Feature extraction and quality control parameters. *Journal of Atmospheric and Oceanic Technology*, **22**, 1105-1113.